Electronic Supplementary Information (ESI) for

Towards decarbonization in transportation: scalable transparent radiative cooling for enhanced vehicle energy efficiency

Min Jae Lee, [a,b] Xuanjie Wang,[c,i] Tae Han Kim, [d] Rohith Mittapally, [c] Won Sik Kim, [e] Young Ko, [c] Bong Jae Lee, [f] Jae Hyun Song, [d] Hyung Jun Lee, [d] Doo Nam Moon, [g] Seung Hwan Ko, *[a,h] Gang Chen*[c]

Corresponding author: maxko@snu.ac.kr and gchen2@mit.edu

Supplementary Text

Theoretical heat transfer analysis of the radiative cooling performance

'Cooling power', identified as the net heat dissipation from a given system, plays a pivotal role in determining the efficacy of passive cooling mechanisms. We developed a 1D steady-state heat transfer model to predict the total cooling power P_{cool} from an optically selective equivalent surface that represented the STRC structure composed of window–air–inner substrate. We defined 'cabin' to refer to this optically selective equivalent surface. This model uses Kirchhoff's law of radiation and assigns effective optical attributes to the cabin, which are essential in computing the thermal radiation emitted through an MIR transparent window, combined with the solar and atmospheric radiation the cabin absorbs. The cabin's base was designed to be thermally isolated from external influences. Consequently, the model assesses the net radiative heat flux, P_{rad}, combined with the non-radiative transfer due to conduction and convection, factored by an effective heat transfer coefficient, h_{eff}. P_{cool} for the STRC structure is then expressed as:

$$P_{cool} = P_{rad} - P_{con} = P_{th} - P_{sun} - P_{amb} - P_{con}$$

Here, we decompose the radiative heat flux, P_{rad} into one outgoing and two incoming heat fluxes. First, the thermal radiation emitted from the equivalent surface was calculated as:

$$P_{th}(T) = \int d\Omega \cos\theta \int_0^\infty d\lambda I_{BB}(T,\lambda)\epsilon(\lambda,\theta)$$

where $\int d\Omega = 2\pi \int_0^{\pi/2} d\theta \sin\theta$ is the angular integral over a hemisphere, and the spectral radiance of a blackbody at temperature T of the equivalent surface is

$$I_{BB}(T,\lambda) = \frac{2hc^2}{\lambda^5} \frac{1}{e^{hc/\lambda k_B T} - 1}$$

where h is Planck's constant, k_B is the Boltzmann constant, c is the speed of light, and λ is the wavelength. Second, the atmospheric radiation absorbed by the equivalent surface was calculated as:

$$P_{atm}(T_{amb}) = \int d\Omega \cos\theta \int_0^\infty d\lambda I_{BB}(T_{amb},\lambda)\epsilon(\lambda,\theta)\epsilon_{atm}(\lambda,\theta)$$

where the surface emittance $\epsilon(\lambda,\theta)$ replaces the surface absorptance $\alpha(\lambda,\theta)$ using Kirchhoff's radiation law. The angle-dependent atmospheric emittance is given by $\epsilon_{atm}(\lambda,\theta) = 1 - t(\lambda)^{1/\cos\theta}$, where $t(\lambda)$ is the atmospheric transmittance at the zenith angle of zero. We leveraged the atmospheric model of U.S. Standard Atmosphere 1976 for $t(\lambda)$. Finally, the solar irradiance absorbed by the equivalent surface was calculated as:

$$P_{sun} = \int d\Omega \cos\theta \int_0^{\infty} d\lambda I_{sun}(\lambda)\epsilon(\lambda)$$

where I_{sun} is the solar irradiance at the zenith angle of zero, in which we used the AM1.5 solar spectra. Summing up, $P_{rad}(T, T_{amb}) = P_{th}(T) + P_{atm}(T_{amb}) + P_{sun}$ is a function of the STRC and ambient temperatures with solar irradiance and atmospheric transmittance depending on the weather conditions. To complete the expression, the non-radiative heat transfer is modeled with an effective heat transfer coefficient, h_{eff} as follows:

$$P_{con} = h_{eff}(T - T_{amb})$$

where P_{con} represents the sum of the heat conduction and convection between the STRC structure and its surroundings. $h_{con} = 10\ W/m^2K$ is assumed to generate modeling predictions presented in this section.

The temperature of the exterior can be calculated using the steady state of $P_{cool} = 0$. In this model, solar illumination and thermal radiation are included to simulate external temperatures with 0.80 emittance of the exterior and an ambient temperature of 30 °C, assuming convection and conduction are negligible.

1D thermal resistance modeling of a car for steady-state and transient analysis

To understand the heat transfer performance of a vehicle under various ambient conditions, we developed a simplified 1D thermal model of a typical vehicle, as shown in Figure S18a. A vehicle is modeled as a black absorbing interior (temperature T_b), separated from an optically translucent window (T_w) through an air gap (temperature T_{air}). The window's optical properties are varied in different cases based on measured spectra. The corresponding thermal resistance-capacitance network is shown in Figure S18b.

To model HVAC heating or cooling via hot/cool air, we introduce a node between the window and the absorber, and apply an energy input, Q_{HVAC}, at the air node. Based on this resistance network, the governing equations are:

$$-C_b\frac{dT_b}{dt} + Q_{solar,2} + \frac{(T_c - T_b)}{R_{rad,in}} + \frac{(T_{air} - T_b)}{R_{conv,in}} = 0$$

$$-C_w\frac{dT_w}{dt} + Q_{solar,1} - Q_{rad,cool} + \frac{(T_b - T_c)}{R_{rad,in}} + \frac{(T_{amb} - T_c)}{R_{ext}} + \frac{(T_{air} - T_c)}{R_{conv,in}} = 0$$

$$Q_{HVAC} - C_{air}\frac{dT_{air}}{dt} + \frac{(T_c - T_{air})}{R_{conv,in}} + \frac{(T_b - T_{air})}{R_{conv,in}} = 0$$

$$R_{ext} = \frac{R_{rad,amb} R_{conv,amb}}{R_{rad,amb} + R_{conv,amb}}$$

Here R_{ext} is the effective thermal resistance outside the vehicle. The radiative cooling power is represented as $Q_{rad,cool}$, while the solar components absorbed in the absorber and the window are $Q_{solar,2}$ and $Q_{solar,1}$. For different films, the absorbed power is computed using their measured optical properties.

Estimation of $R_{conv,in}$:

The convective heat transfer coefficient for free convection between two parallel plates, relevant to the air gap between the window and the absorber is estimated as[1],

$$R_{conv,ll} = \frac{L}{2Nu_L kA}$$

$$Nu_L = 1 + 1.44\left(1 - \frac{1708}{Ra_L \cos\beta}\right)\left[1 - \frac{1708(sin1.8\beta)^{1.6}}{Ra_L \cos\beta}\right] + \left[\left(\frac{Ra_L cos\beta}{5830}\right)^{1/3} - 1\right]$$

$when\ Ra_L > {}^{1708}/_{cos\beta}; otherwise\ Nu_L = 1$

Here, L is the air gap thickness, k is the thermal conductivity of air, A is the area of the system, $\beta\ (= 10°)$ is the angle measured from the earth's surface, and Ra_L is the Rayleigh number corresponding to the gap L. To account for enhanced convective heat transfer due to mixing, a fitting parameter a is introduced, and the convective resistance is calculated as $R_{conv,in} = aR_{conv,ll}$.

Estimation of $R_{conv,amb}$:

The external convective resistance is calculated using standard correlations for natural and forced convection[2]:

$$R_{conv,amb} = \frac{W}{Nu_w kA}$$

$$Nu_w = \begin{cases} 0.54Ra_w^{1/4} & if\ u = 0\ and\ T_w > T_{amb} \\ 0.52Ra_w^{1/5} & if\ u = 0\ and\ T_w < T_{amb} \\ 0.037Re_w^{4/5} Pr^{1/3} & if\ u > 0 \end{cases}$$

Here, W is the width of the vehicle, u is the wind velocity, and Re, Pr are the Reynolds and Prandtl numbers, respectively.

Estimation of radiative heat transfer coefficients:

Radiative thermal resistances depend strongly on the window's optical properties. For the BE/BA case, the window is strongly emissive in the mid-infrared, and thus exchanges radiation with the absorber, ambient, and outer space. For the low-e case, the window is modeled as highly reflective—i.e., having negligible emissivity in the infrared—and therefore does not exchange thermal radiation with any other component.

For BE/BA windows:

$$R_{rad,in} = \frac{(1/\varepsilon_b + 1/\varepsilon_w - 1)}{\sigma A (T_b + T_w)(T_b^2 + T_w^2)}$$

where $\varepsilon_b = 1, \varepsilon_w = 1$

For the ambient:

$$R_{rad,amb} = \frac{1}{(\varepsilon_{atm}\sigma(T_w + T_{amb})(T_w^2 + T_{amb}^2))}, \varepsilon_{atm} = 0.7$$

For low-e windows, radiative exchange is neglected and only convective resistances apply.

Finally, the radiative cooling is expressed as:

$$Q_{rad,cool}(T_w) = \int d\Omega \cos\theta \int_{8\,\mu m}^{13\,\mu m} d\lambda I_{BB}(T_w, \lambda)\epsilon(\lambda, \theta)$$

where $\int d\Omega = 2\pi \int_0^{\pi/2} d\theta \sin\theta$ is the angular integral over a hemisphere, and the spectral radiance of a blackbody at surface temperature T is

$$I_{BB}(T, \lambda) = \frac{2hc^2}{\lambda^5} \frac{1}{e^{hc/\lambda k_B T} - 1}$$

Here, h is Planck's constant, k_B is the Boltzmann constant, c is the speed of light, λ is the wavelength of light. Integrating over the 8–13 μm window gives: $Q_{rad,cool}(T_c) \approx 0.27\sigma T_c^4$

Steady-state analysis: To evaluate vehicle thermal performance under steady conditions, we fix T_{air} at a comfort level (22 °C) and solve the system using MATLAB for the temperatures and Q_{HVAC}. Results for three cases—STRC film, base case, low-e—as a function of ambient temperature are shown in Figure 5A.

Transient analysis: The transient model is used to simulate the vehicle's thermal response in summer and winter. HVAC power density is modified as:

$$Q_{HVAC}\left(1+\frac{T_{air}-T_{HVAC}}{T_{air,i}-T_{HVAC}}\right)$$

where $T_{air,i}$ is the initial cabin temperature, and T_{HVAC} is set to 10 °C (cooling) and 60 °C (heating), based on experimental inputs. The total HVAC energy consumed to reach steady state is shown in Figures 5B and 5C.

Theoretical 2-D heat transfer analysis of the radiative cooling performance

We developed a 2D computational model using commercial finite-element software (COMSOL 6.1) to characterize the steady state temperature profile inside the cabin considering heat conduction, convection, and thermal radiation. The model comprised the STRC sample, air cabin, solar absorber, and aluminum-covered thermal insulations. The geometry and dimensions in the computational model were the same as the experimental setup. The semitransparent conditions were applied to the top and bottom surfaces of the sample considering optical transmittance, reflection, and absorption based on measurements. The diffuse conditions were applied to the solar absorber surface and aluminum-coated inner walls with measured optical properties. For the outside surface, the incoming solar irradiation, surface reflectance, sky atmospheric window (wavelength range from 8–13 μm), and natural convection between the cabin and ambient were all considered.

Optical simulation model for optimizing the STRC structure.

PMMA layer

In the proposed STRC structure, the topmost PMMA layer served as an MIR emitter. Supplementary Fig.4 shows the calculated normal emittance of a freestanding PMMA film 100 μm thick using the ray-tracing method. In the calculation, we used the optical constants of PMMA that were measured by using an ellipsometer (VASE and VASE II). As noted from Supplementary Fig.4, 100 μm thick PMMA can serve as an excellent MIR emitter, especially in the atmospheric transparent window (approximately 8–13 μm). To examine the effect of PMMA's thickness on the MIR emittance, Supplementary Fig.3C shows the normal emittance in the range of 20–200 μm. It is evident that 100 μm can be considered as being sufficiently thick to boost the emittance value by approximately l–12 μm.

SiO_2 layer

In the proposed STRC structure, the bottommost glass (i.e., windshield of a car) serves as a broadband absorber. Since the ITO/Ag/ITO/PET multilayer structure is opaque in the MIR spectral region, MIR emission from the glass cannot contribute to the radiative cooling performance.

Rather, it absorbs the spontaneous radiation from the cabin and transfers its thermal energy via heat conduction to the upper layers (PMMA layer) so that MIR emission from the PMMA layer increases. Supplementary Fig.8 shows the calculated absorptance of 2.1 mm glass using the ray-tracing method with the measured optical constants using an ellipsometer. Because the windshield of a car is of the order of millimeters thick, it indeed functions as an effective broadband absorber.

ITO/Ag/ITO layers

In the proposed STRC structure, the ITO/Ag/ITO layers served as an NIR reflector that rejected the undesirable portion of solar radiation back to the outside space. Supplementary Fig.10 shows the contour plot of the reflectance, transmittance, and absorptance of a freestanding ITO/Ag/ITO layer as a function of Ag and ITO thicknesses using thin-film optics[3]. In the calculation, we used the measured optical constants for ITO using an ellipsometer (IR-VASE) and the Drude model considering the size effect[4] for Ag. To demonstrate the wavelength-selective functionality of the ITO/Ag/ITO layers, we calculated arithmetically-averaged values in two different spectral regions, one from 400–700 nm (visible region) and the other from 1200–2500 nm (NIR region). The objective was to find a configuration that maximized both the visible transmittance and the NIR reflectance. Supplementary Fig.10 shows that the thicknesses of Ag and ITO induce opposite effects on visible transmittance and NIR reflectance; that is, as the Ag and ITO layers get thinner, the visible transmittance increases, however, the NIR reflectance decreases. Therefore, an optimum condition exists that maximizes both the visible transmittance and the NIR reflectance. From the analysis, we have determined the thickness of Ag and ITO to be 10 and 65 nm, respectively.

Vehicle and thermal comfort simulation

Full vehicle

The vehicle cooling performance was verified using a coupling process of 3 tools (GT, TAITherm, and StarCCM+), and this wasF then used to verify the occupant comfort. Simulation calculations were performed for components such as the evaporator, condenser, and compressor using the 1D system model. A 3D model was used to verify the vent temperature according to the discharge air volume for each mode (Vent, Floor) and the temperature following door opening. Each verified system was integrated and coupled, and full vehicle verification was conducted using a 3D system model. Coupling data exchange was as follows.

- 3D system (surface temperature) ↔ 3D CFD (convection data)
- 1D system (heat exchanger heat rate) ↔ 3D CFD (heat exchanger temperature/speed)

CoTherm software was used to automatically perform coupling, according to user-defined parameters such as scenario, parts requiring coupling, and data exchange cycle. For RG3, the test-analysis errors showed cooling (surface 0.58 ℃/air 0.76 ℃) and heating (surface -1.59 ℃/air 1.76 ℃).

Thermal comfort

We used TAITherm's Human Thermal Extension software to evaluate the human body's physiological response and comfort in the cabin environment. The human body was modeled using multiple layers of physiological tissue and clothing layers. Clothing characteristics, air speed, temperature, solar radiation, activity level, and activity type were used as boundary conditions. Air velocity and temperature were obtained through coupling analysis, and solar radiation was obtained from weather data. Customization was required for the remaining clothing characteristics and activity levels/types. The analysis included physiological responses such as skin tremors, sweating, and vasomotor activity, and calculated average and local temperatures for the skin and core. These physiologically-based temperatures were used in the Berkeley Thermal Comfort model to calculate the thermal sensation and thermal comfort at both whole body and local levels.

CO_2 reduction and energy saving performance calculation.

Using experimental data from both the STRC and basic sedan automobiles, an analysis of the yearly vehicle A/C energy usage was conducted in this study. The daily amount of energy used for A/C when driving was calculated by multiplying the A/C consumption by the US average driving time[5]. To get the yearly vehicle A/C demand, this was then multiplied by the number of summer days in each state that were over 65 °F[6]. Four US-representative areas were chosen for comparison: the West, South, Midwest, and Northeast.

$$\frac{A/C\ consumption\ (kwh)}{vehicle\ \cdot year} = \text{A/C consumption (wh)} \times \text{driving time} \times \text{A/C working day over 65 °F}$$

We used a particular methodology to estimate the annual CO_2 emissions from passenger cars in the US[7]. First, to calculate the annual gasoline consumption of each car, we multiplied US annual traveled mileage[8] by the US average fuel efficiency[9]. We then multiplied this number by the CO_2 emissions generated for every gallon of fossil fuel consumed[10]. Lastly, the total CO_2 emissions were calculated using the ratio of the methane and nitrous oxide emissions to the total CO_2 emissions from cars. We used state-level vehicle miles traveled data and created a color-coded map to better depict our findings.

$$\frac{\text{Total CO2}\ \ kg}{year}$$

Furthermore, we calculated the annual driving distance saved for both STRC and normal vehicles. The US average EV fuel economy data[11] and number of vehicles by state[12] were multiplied by the annual A/C energy consumption use that we calculated above. Fuel efficiency was multiplied by the annual gasoline consumption and by the total trip distance for each state for both STRC and base vehicle. Our calculated total CO_2 emission was within 0.1% accuracy compared to total CO_2 emission of 1,488 Megatons by US Energy Information Administration[13].

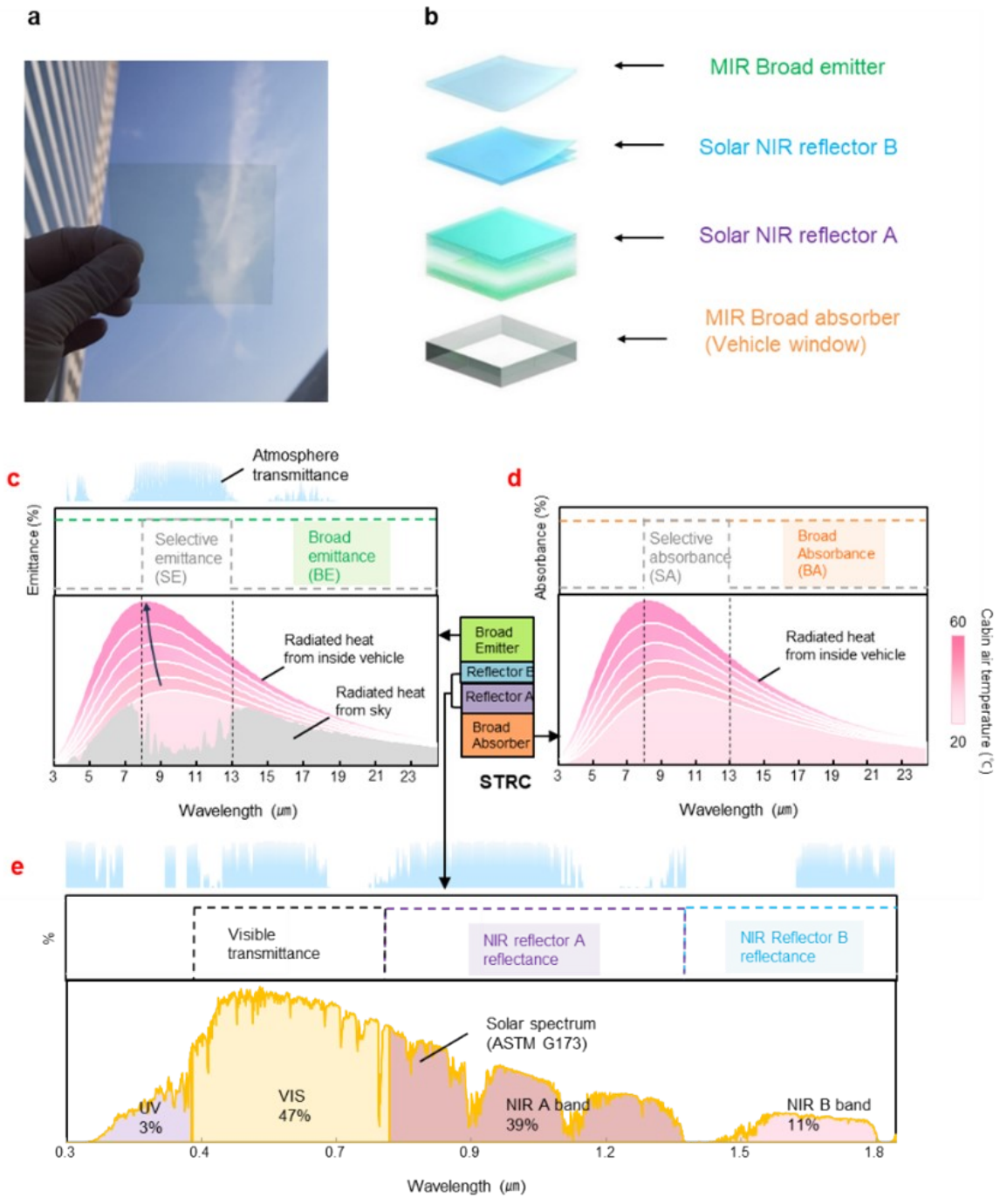

Fig. S1. Principle and design of STRC film for vehicle thermal management (a) Photo of STRC sample. (b) Schematic structure of optical properties for STRC (c) Blackbody radiation spectra correspond to cabin air temperatures between 20 and 60 °C (red shaded area) and to the radiated sky (gray shaded area). In typical radiative cooling applications, a selective emitter (SE) is used to maximize emission within the atmospheric transparency window while minimizing emittance in the rest of the mid-IR range to reduce heat gain from the ambient. In contrast, parked vehicles are usually hotter than the ambient air and therefore require a broadband emitter (BE) that can radiate effectively to both the sky and the surroundings. (d) To radiative heat from cabin (red

shaded area for cabin temperature from 20 to 60 ℃), the interior surface should also be broad absorber (BA) (e) Visible transmittance and NIR reflection via the solar spectrum with energy distribution. The atmosphere transmission spectrum covers the UV to MIR wavelength range.

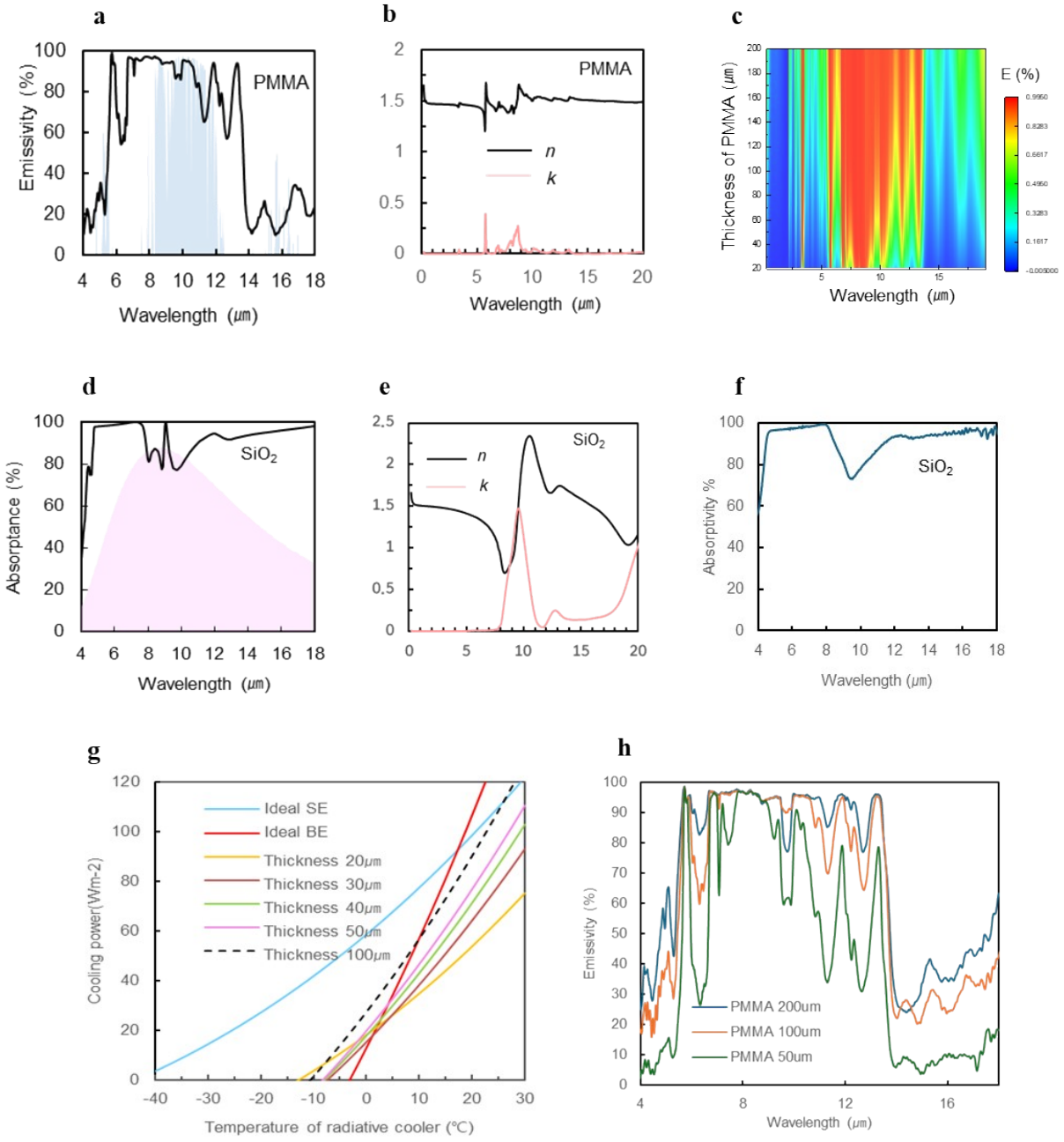

Fig S2. Optical properties of STRC in each layer (a) Calculated MIR emittance spectrum of a broad emitter with a thickness of 100 μm. (b) Measured optical constants *n*, *k* of PMMA. (c) Calculated emittance of PMMA as a function of MIR wavelength for different thicknesses. (d) Calculated MIR emission spectrum of a broad absorber with a thickness of 2.1 mm. (e) Measured *n*, *k* of SiO_2 (c) Measured absorptance of 2.1 mm SiO_2. (g) Cooling power of PMMA for different thicknesses compared with ideal BE. As thickness increases, its cooling power approaches to ideal BE cooling power. (h) Measured emission of PMMA varying thicknesses.

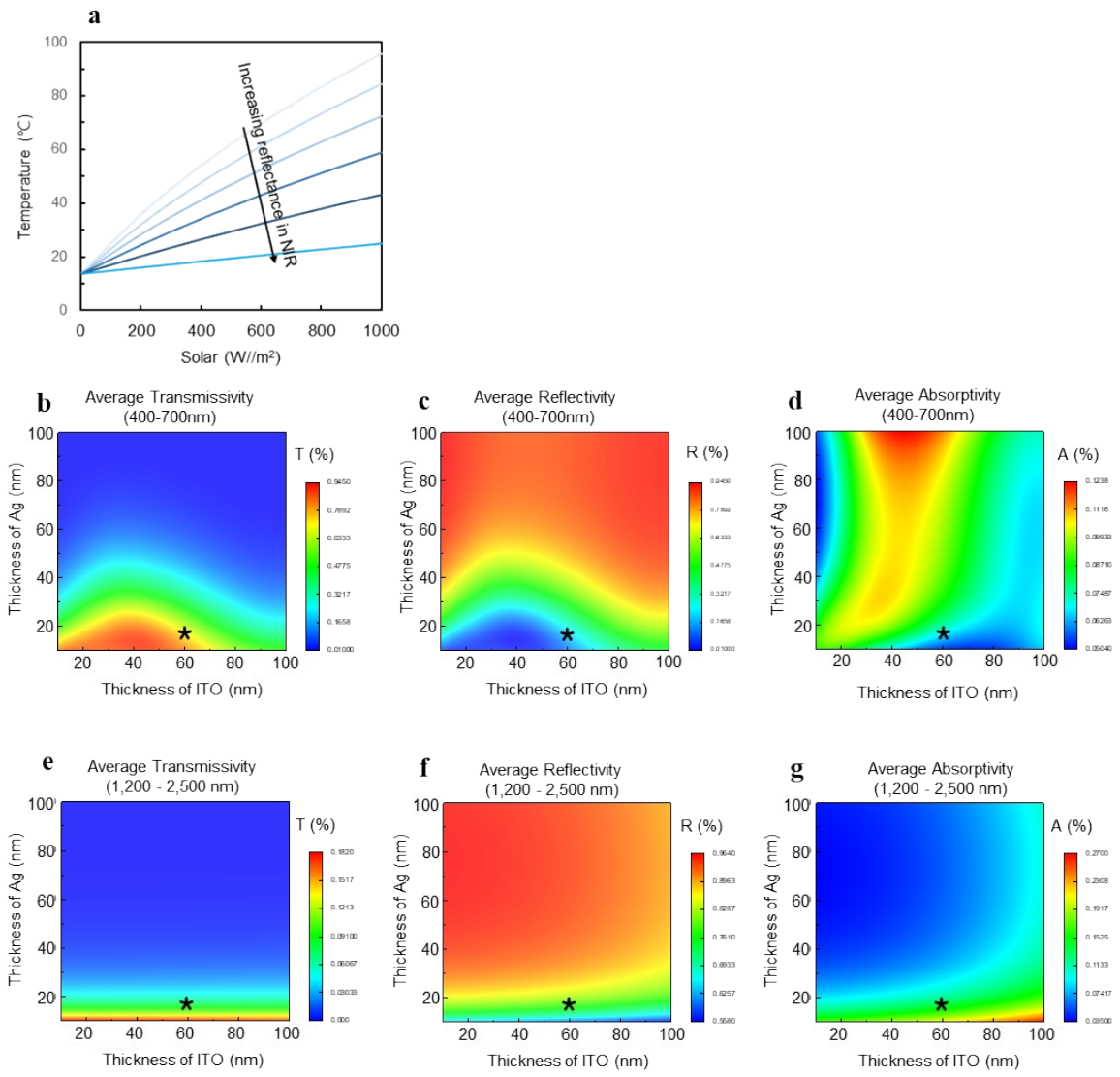

Fig. S3. (a) Calculated temperature varying solar intensity increasing reflectance in NIR 1,200 – 2,000 nm wavelength region. (b) Calculated optical properties of ITO/Ag/ITO for different thicknesses for each layer. Average transmittance in visible spectrum. (c) Average reflectance in visible spectrum. (d) Average absorption in visible spectrum. (e) Average transmittance in NIR spectrum. (f) Average reflectance in NIR spectrum. (g) Average absorption in NIR spectrum. Asterisk symbol indicates actual thicknesses for STRC fabrication.

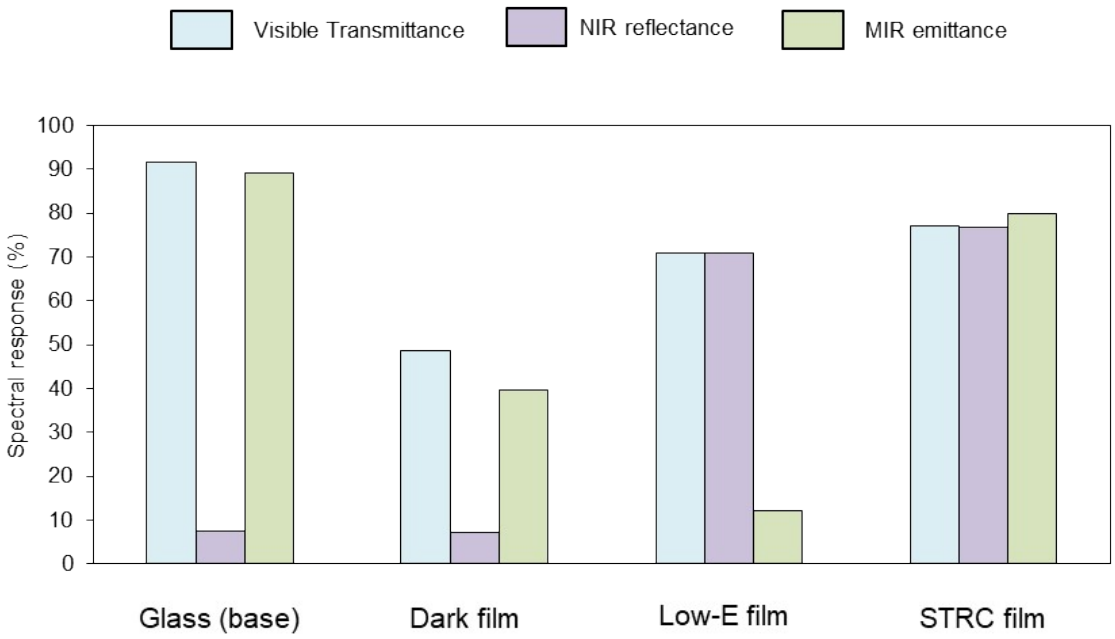

Fig. S4. Measured average optical properties of glass, commercial dark film, commercial Low-E film and STRC film exhibiting similar average transmittance in the visible range and reflectance in the NIR range while exhibited different emittance in the MIR range

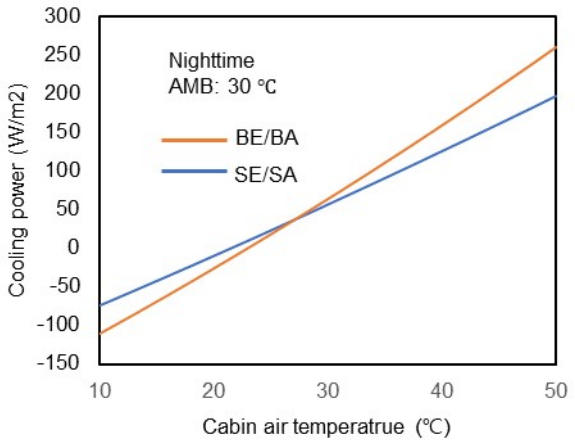

Fig. S5. Calculated cooling power of BE/BA and SE/SA for different cabin temperatures at night.

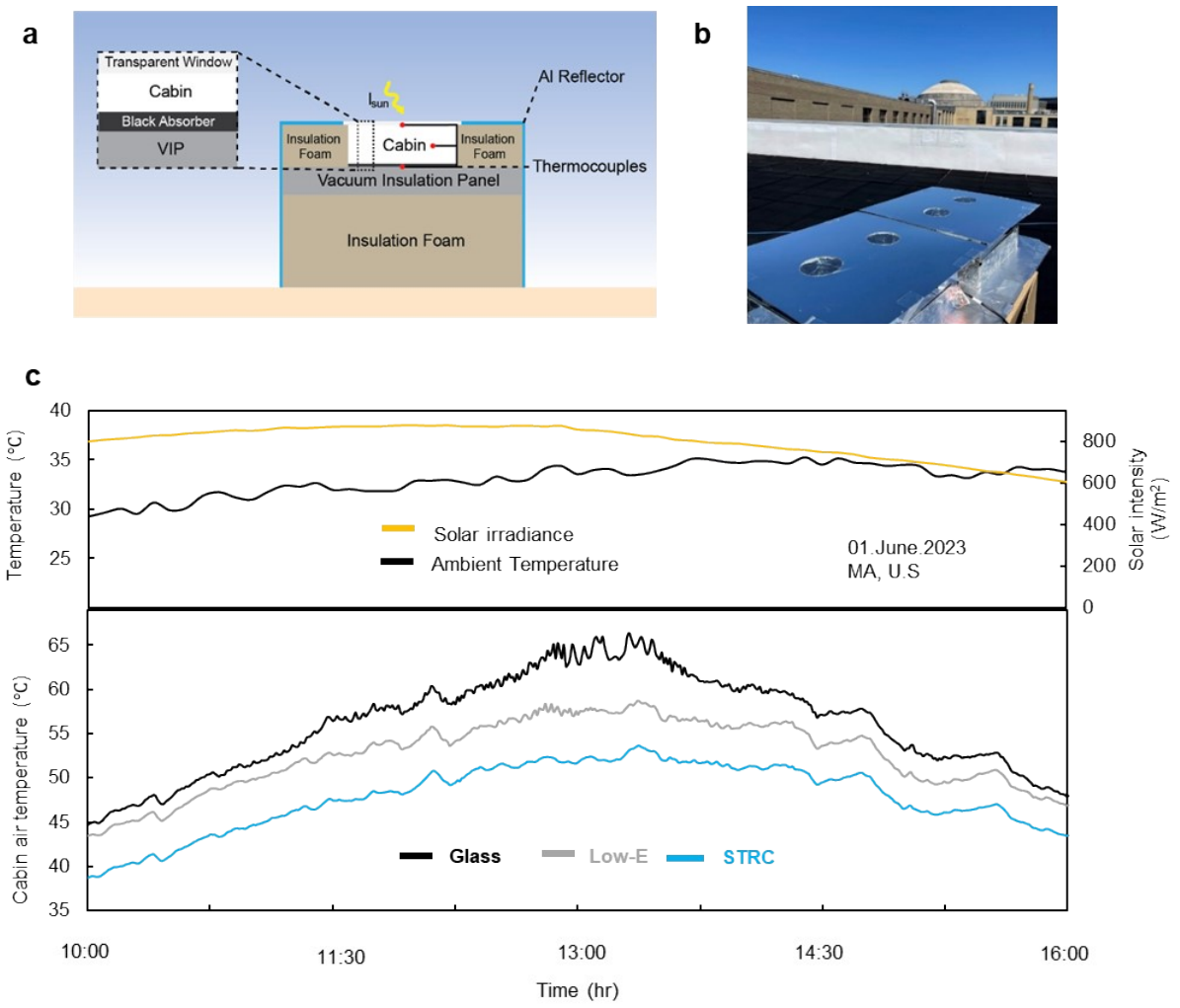

Fig. S6. Cooling performance characterization using a test cabin. (a) Schematic and (b) Photograph of the experimental setup used to characterize radiative cooling performance. (c) Measured cabin air temperature, solar irradiance, and ambient temperature for three different samples over 8 h in Massachusetts, U.S, June 1, 2023.

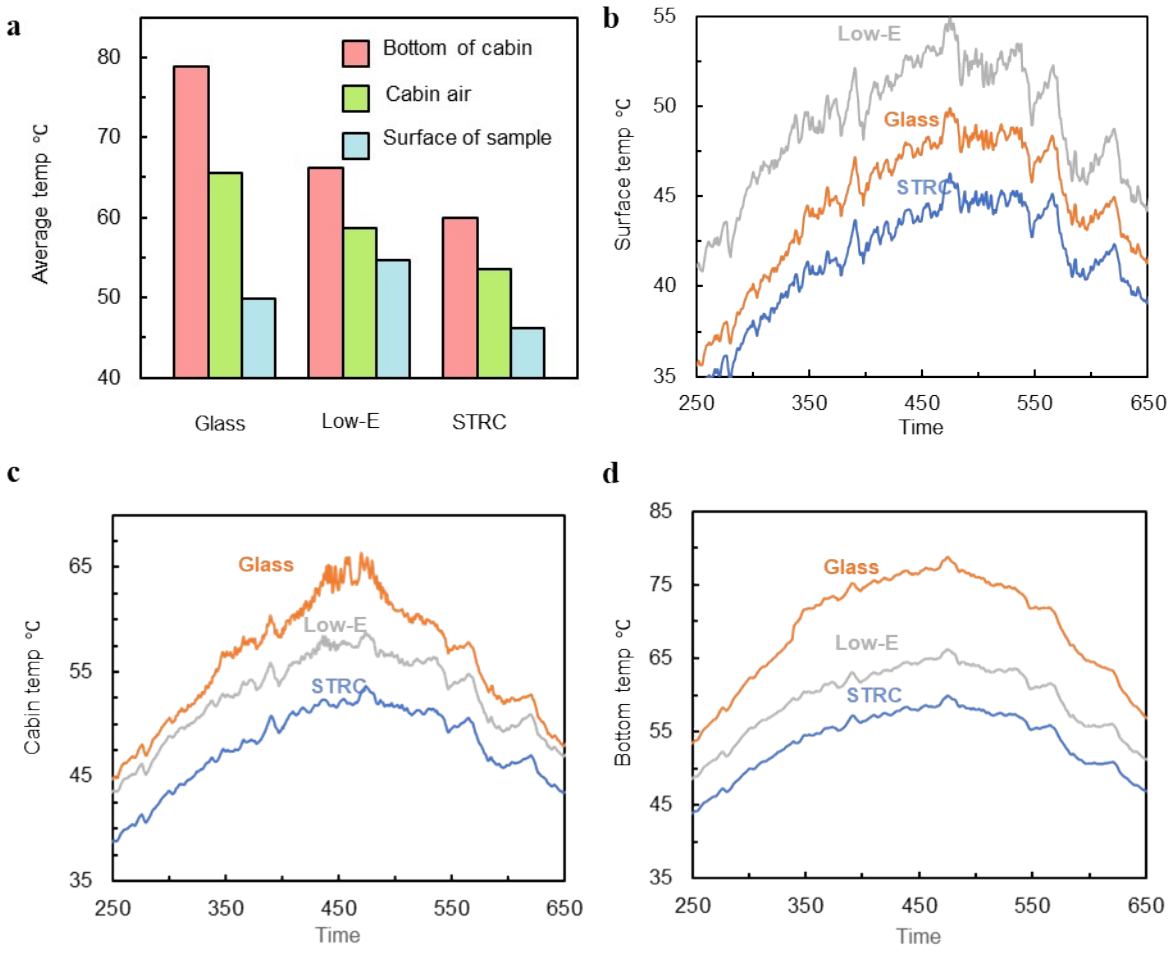

Fig. S7. Measured temperature of three samples. (a) Average temperature of each sample in bottom, air, and top. (b) Surface temperature of three samples. (c) Cabin air temperature of three samples. (d) Bottom surface temperature of three samples.

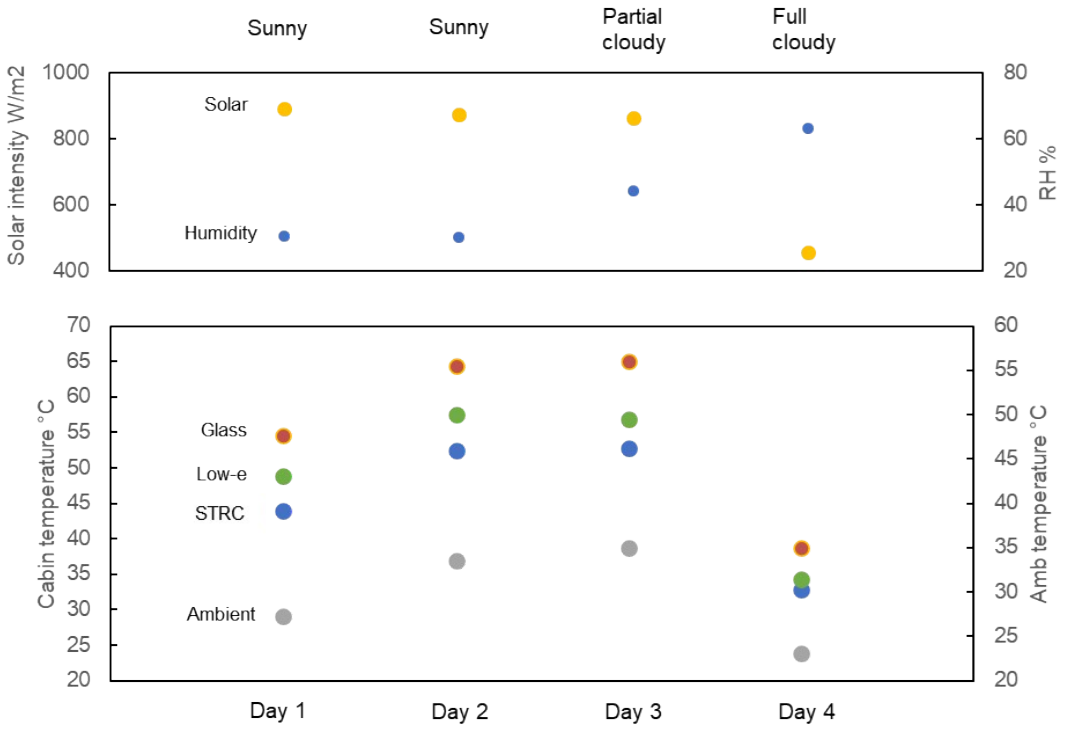

Fig. S8. Measured cabin air temperature of three samples in different weather conditions.

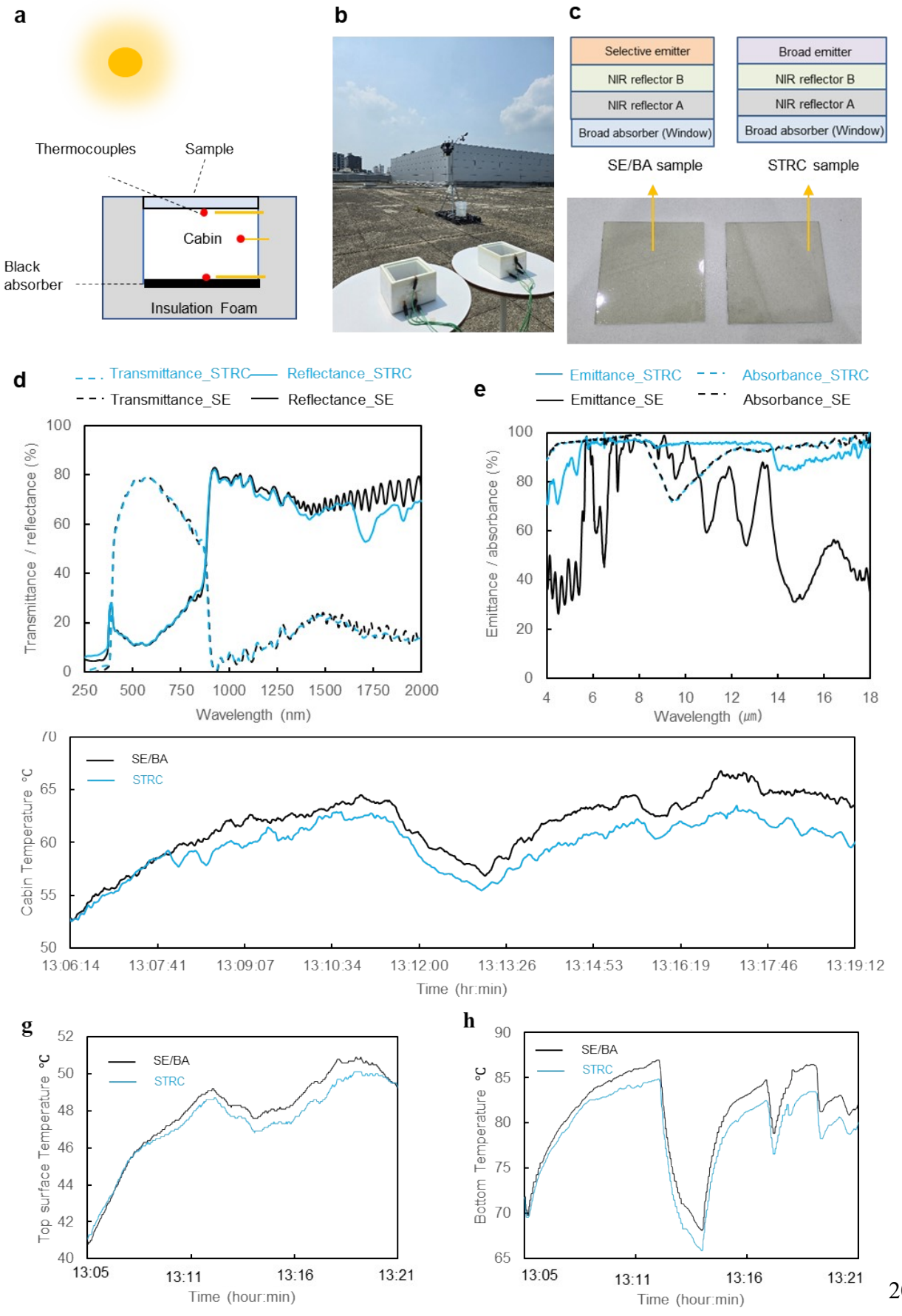
a
Thermocouples
Sample
Cabin
Black absorber
Insulation Foam
b
c
Selective emitter
NIR reflector B
NIR reflector A
Broad absorber (Window)
Broad emitter
NIR reflector B
NIR reflector A
Broad absorber (Window)
SE/BA sample
STRC sample
d
Transmittance_STRC
Reflectance_STRC
Transmittance_SE
Reflectance_SE
Transmittance / reflectance (%)
Wavelength (nm)
e
Emittance_STRC
Absorbance_STRC
Emittance_SE
Absorbance_SE
Emittance / absorbance (%)
Wavelength (㎛)
SE/BA
STRC
Cabin Temperature °C
Time (hr:min)
g
Top surface Temperature °C
Time (hour:min)
h
Bottom Temperature °C
Time (hour:min)

Fig. S9. Measured performance comparison between STRC and SE sample. (a) Schematic view of experimental setup (b) Photo of experimental setup and samples structures (c-d) Measured optical properties of STRC and SE sample in UV-VIS range, and MIR range (e-g) Measured cabin, top, and bottom temperature of STRC and SE sample at ambient 34℃ with solar radiation 980W/m^2 condition.

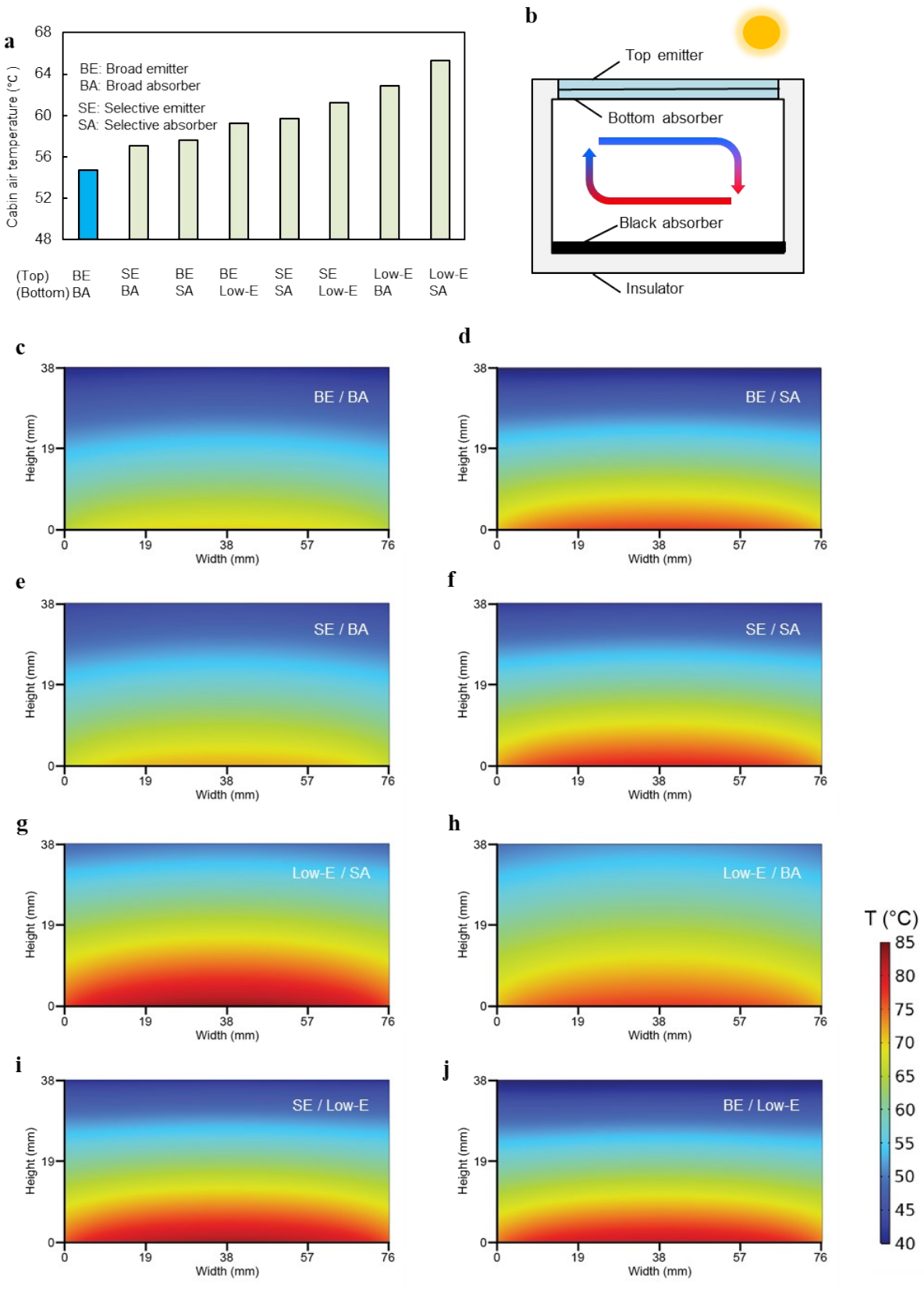
a
Cabin air temperature (°C)
68
64
60
56
52
48
BE: Broad emitter
BA: Broad absorber
SE: Selective emitter
SA: Selective absorber
(Top) BE SE BE BE SE SE Low-E Low-E
(Bottom) BA BA SA Low-E SA Low-E BA SA
b
Top emitter
Bottom absorber
Black absorber
Insulator
c
BE / BA
d
BE / SA
e
SE / BA
f
SE / SA
g
Low-E / SA
h
Low-E / BA
i
SE / Low-E
j
BE / Low-E
Height (mm)
Width (mm)
0
19
38
57
76
T (°C)
85
80
75
70
65
60
55
50
45
40

Fig. S10. Simulated test cabin air temperature profile with different combinations of top emitter and bottom absorber using same ideal optical properties in range (300 – 2,000nm), but different optical properties in range (4-20 μm). (a) Cabin air temperature results using various combinations of ideal optical properties at the top and bottom, with the BE/BA (STRC) combination reaching the lowest cabin temperature. (b) Schematic view of theoretical analysis on heat transfer in cabin. (c) BE/BA case (d) BE/SA case (e) SE/BA case (f) SE/SA case (g) Low-E /SA case (h) Low-E /BA case (i) SE /Low-E case (j) BE /Low-E case.

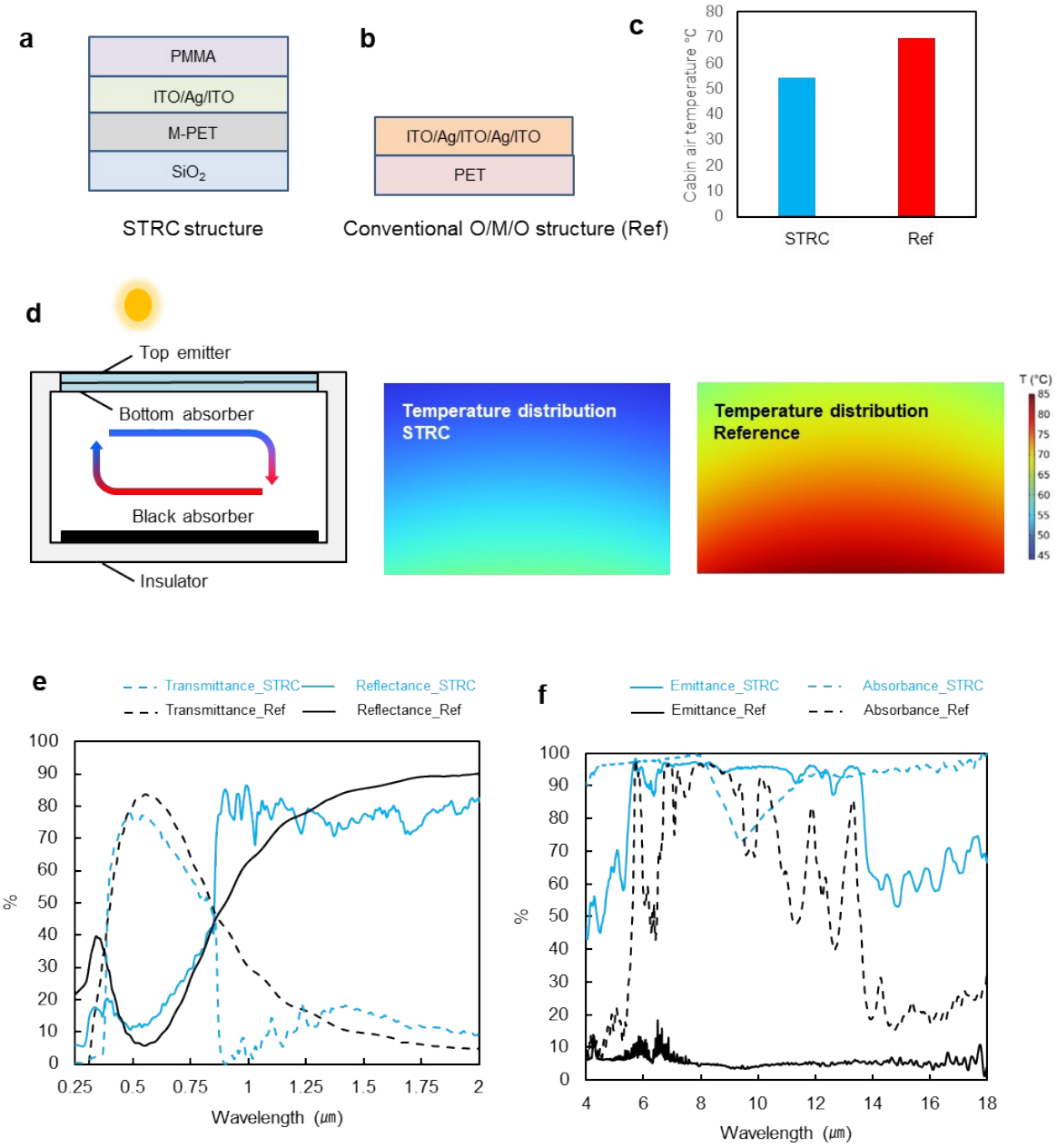

Fig. S11. Performance comparison between STRC and conventional Oxide/Metal/Oxide structure. (a) structure of STRC (b) structure of conventional O/M/O structure. (c-d) Calculated cabin temperature comparison. (e-f) Measured optical properties of STRC and conventional O/M/O structure

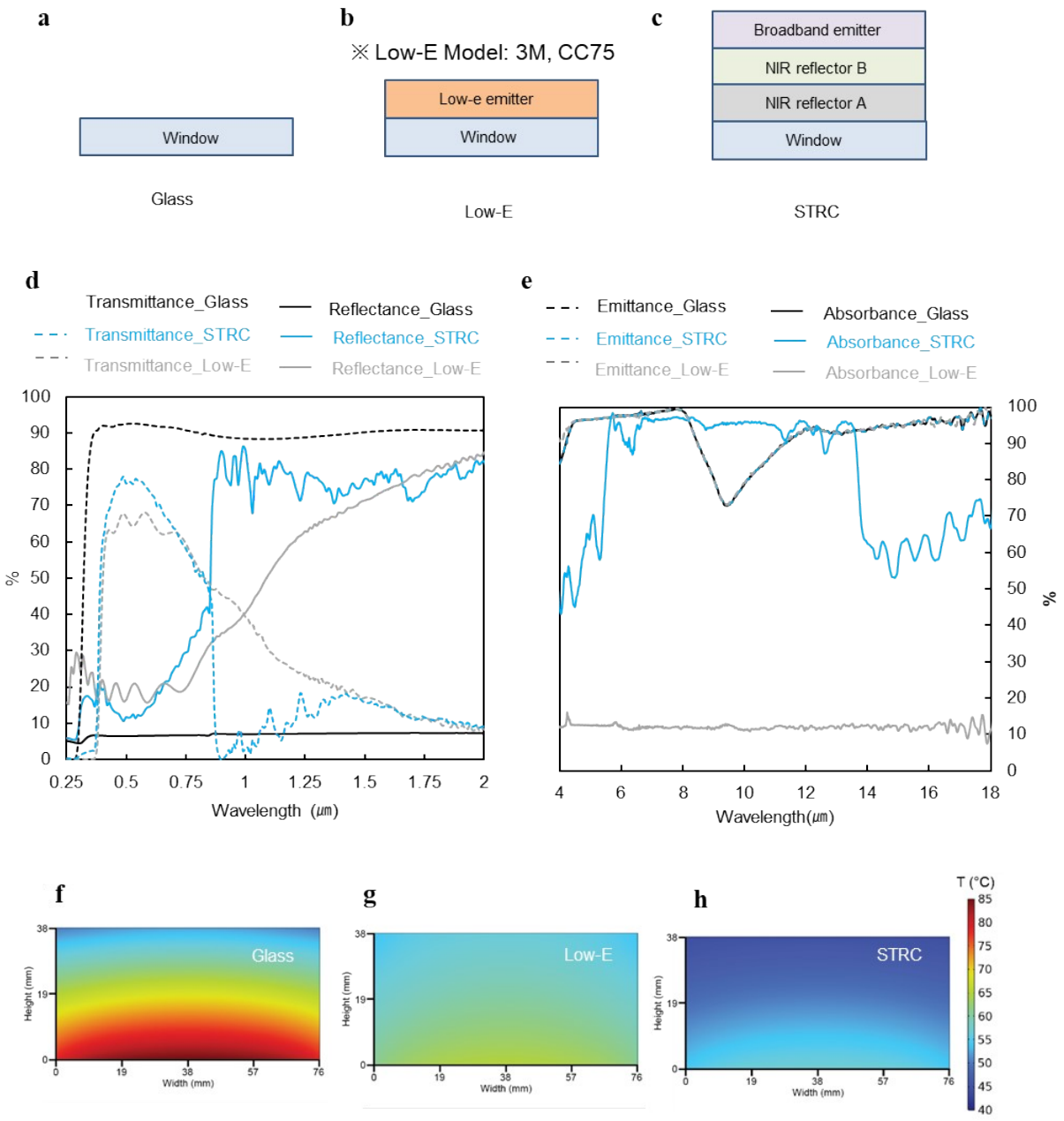

Fig. S12. Structure of three samples for experimental measurements. (a) Clear vehicle window. (b) Low-E film[59] laminated on clear vehicle window. (c) STRC film laminated on clear vehicle window. (d) Transmittance (dotted line) and reflectance (solid line) of three samples in solar spectrum range. (e) Emittance of three samples in MIR spectrum. Simulated cabin air temperature profile using measured optical properties of (f) Glass on top (g) STRC on top (h) Low-E on top.

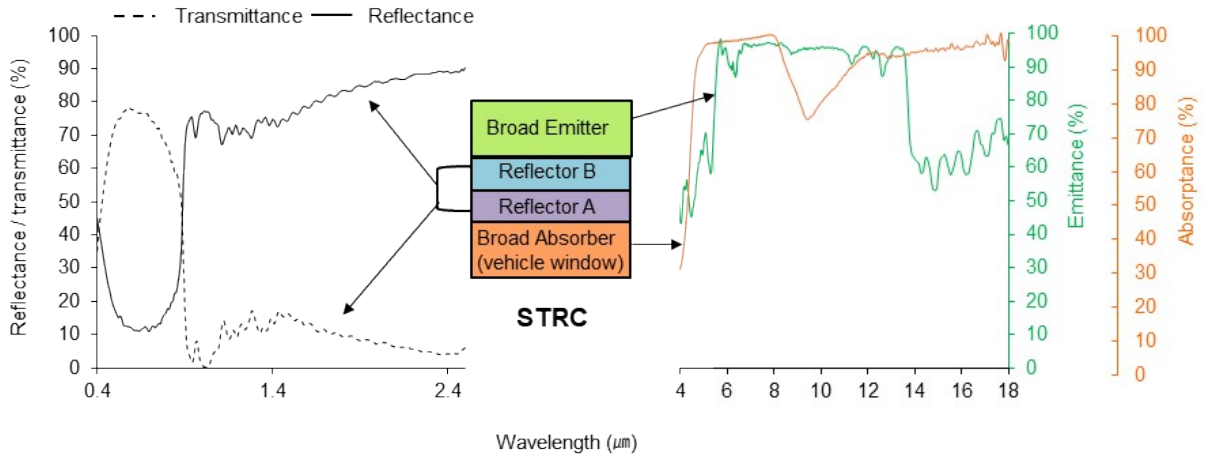

Fig. S13. Measured STRC on 2.1 mm vehicle glass of transmittance/reflectance (dotted line/ solid line) in the visible and NIR regions from 0.3 to 2.4 µm, and emittance/absorbance (green /orange) in the MIR region from 4 to 18 µm.

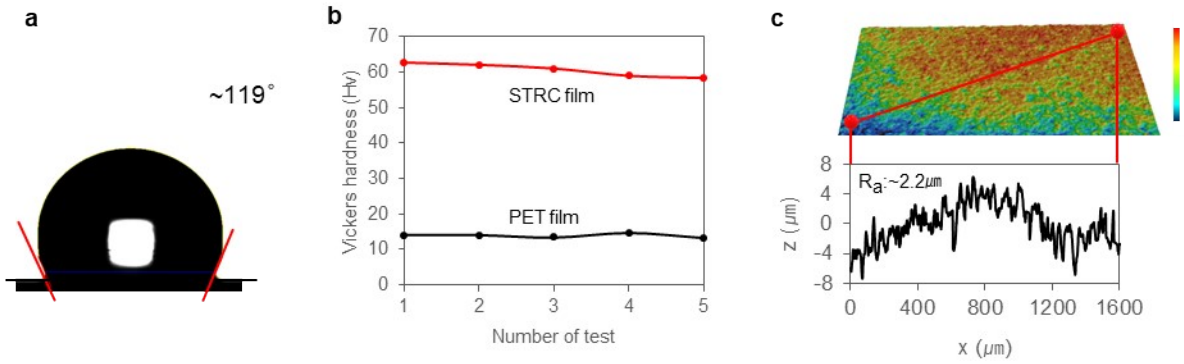

Fig. S14. (a) A photo of a water droplet on a STRC film's surface with a measured contact angle ~119°. (b) Measured hardness of TRPC film compared with commercial PET film (c) Measured STRC film's averaged surface roughness ~2.2 µm.

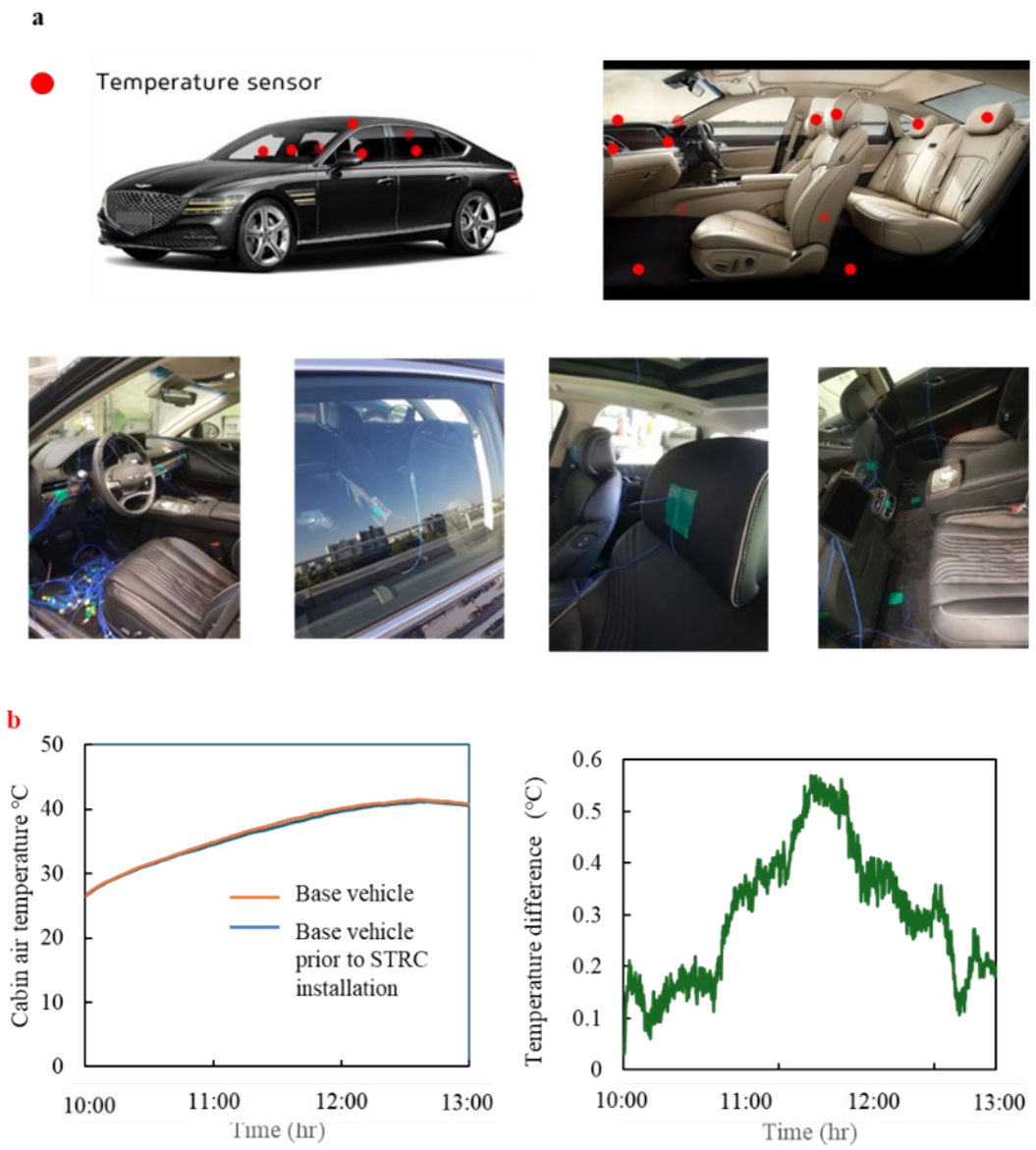

Fig. S15. (a) Locations of thermocouples in vehicles. (b) (Left) Validation of temperature measurement consistency of two base vehicles prior to STRC film installation on the glasses (Right) Temperature difference in the two base vehicles.

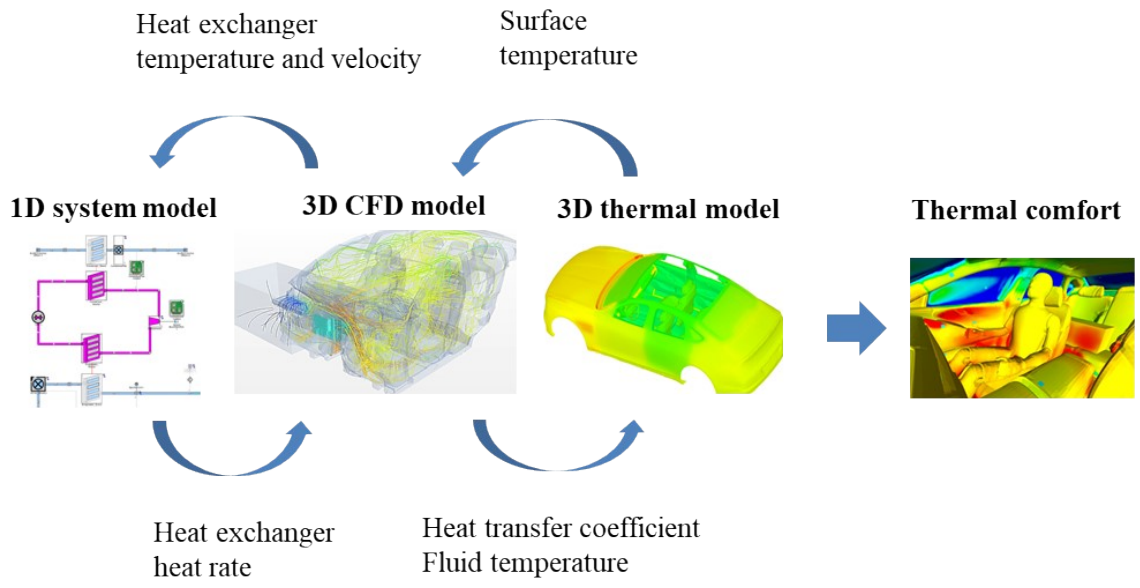

Fig. S16. Vehicle and thermal comfort simulation methodology

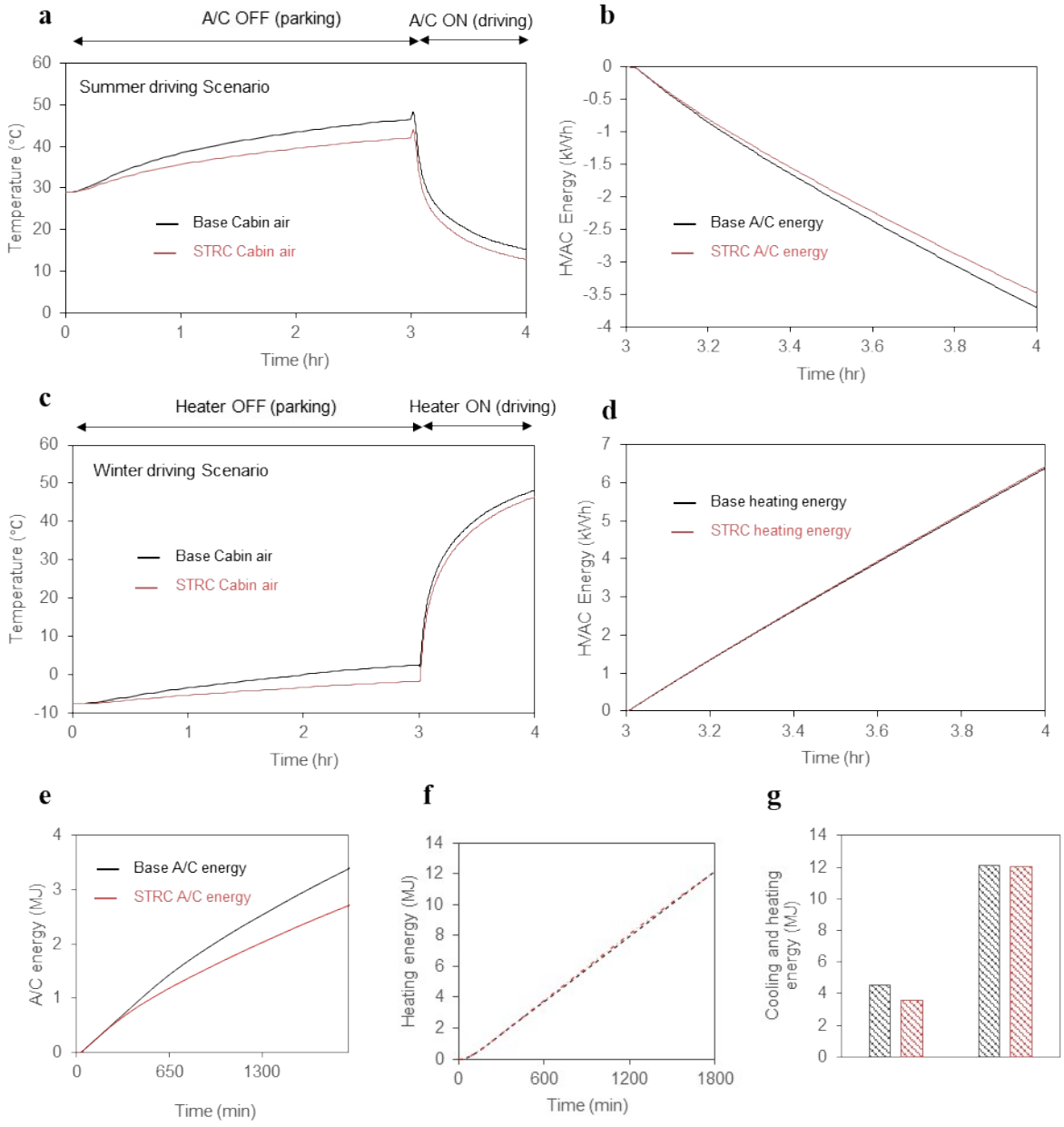

Fig. S17. Full three-dimensional vehicle simulation results in driving state under summer and winter (a) Cabin temperature. Turns A/C off for 3 hours thermal soaking at parking and turns A/C on at driving 50km/h (b) A/C energy consumption at driving (c) Cabin temperature. Turns heater off for 3 hours thermal soaking at parking and turns heater on at driving 50km/h (d) heater energy consumption at driving (e) Accumulated A/C energy consumption. (f) Accumulated heater energy consumption. (g) Accumulated A/C and heating energy consumption comparison.

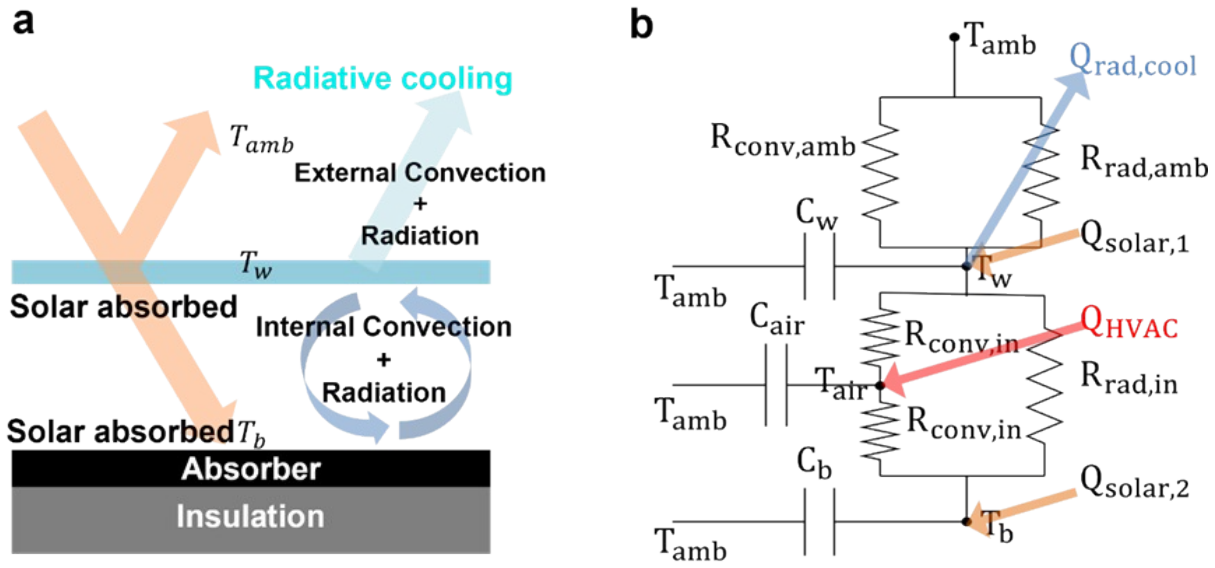

Fig. S18. (a) Simplified 1D model of a vehicle (b) 1D thermal resistance-capacitance network indicating the temperatures, energy fluxes and the thermal capacitances associated with a vehicle.

℃

	BASE sedan	STRC sedan	ΔT	BASE SUV	STRC SUV	ΔT
Cabin air	36.1	33.0	3.0	33.9	31.7	2.3
Front glass	45.8	39.0	6.8	44.8	38.8	6.0
Left glass	40.6	35.9	4.7	38.4	35.2	3.2
Right glass	37.2	33.4	3.9	35.3	32.9	2.5
Rear glass	47.2	41.5	5.7	38.0	34.7	3.3
Roof glass	0.0	0.0	0.0	54.1	44.4	9.7

Table S1. Vehicles thermal comparison test results in Namyang Korea.

℃

	Cabin air	Front glass in	Front glass out	Sunroof in	Sunroof out
BASE sedan	43.0	61.1	54.6	60.1	56.6
STRC sedan	41.3	53.2	49.0	48.9	46.1

Table S2. Vehicles thermal comparison test results in California, U.S

°C

	Cabin air	Breath level	Foot level	Front glass in	Sunroof in
BASE sedan	48.1	52.9	38.5	56.1	68.9
STRC sedan	42.6	45.6	36.6	50.4	58.6

Table S3. Vehicles thermal comparison test results in Lahore, Pakistan

References

S1 Kreith, F. K., J. F. *Principles of Solar Engineering; Hemisphere Publishing Corporation*. (1978).

S2 F. P. Incropera, A. S. L., T. L. Bergman, D. P. DeWitt. *Principles of Heat and Mass Transfer 7th Ed*. (Wiley, 2011).

S3 Zhang, Z. M. *Nano/Microscale Heat Transfer*. Vol. 410 (Springer, 2007).

S4 Kim, D.-m., Nam, J. & Lee, B. J. Plasmon thermal conductivity of thin Au and Ag films. *Physical Review B* 108, 205418, doi:10.1103/PhysRevB.108.205418 (2023).

S5 Steinbach, R. T., B.C. *American Driving Survey: 2022*. (AAA Foundation for Traffic Safety, 2023).

S6 *Daily Climate Normals (1991 - 2020)*. (National weather service).

S7 *Inventory of U.S. Greenhouse Gas Emissions and Sinks: 1990-2021. Chapter 3 (Energy) Tables 3-13, 3-14, and 3-15.*, Vol. EPA #430-R-23-001 (PDF) (Environmental Protection Agency, 2023).

S8 *Average Annual Miles per Driver by Age Group*. (Federal Highway Administration, 2022).

S9 *Highway Statistics Series, Highway Statistics 2020. Office of Highway Policy Information, . Table VM-1.*, (Federal Highway Administration, 2020).

S10 *Tailpipe Greenhouse Gas Emissions from a Typical Passenger Vehicle*. Vol. EPA-420-F-23-014 (Environmental Protection Agency, 2023).

S11 *Comparison: Your Car vs. an Electric Vehicle*. (Environmental Protection Agency, 2023).

S12 *2022 Light-Duty Vehicle Registration Counts by State and Fuel Type*. (Department of Energy).

S13 *How much carbon dioxide is produced from U.S. gasoline and diesel fuel consumption?* , (Energy Information Administration).